# Multi-Scale Thermal Modelling of Composite Material

A.SAAFI, A.MORSY
Instructor: Prof. Polifke
*Technische Universität München, Garching, Allemagne*

**Abstract**
This project explores the thermal management of anisotropic composite material. The motivation is to protect sensitive electronic components from localized heat accumulation during use. The protection of these devices is particularly important, particularly in space applications where vacuum environments limit convective cooling. The project is divided into two strategic phases ; Phase 1 focuses on multiscale homogenization to replace complex heterogeneous microstructures with a validated conductivity tensor, enabling simulations while maintaining physical accuracy. Phase 2 uses this homogenized model to perform numerical experiments. The later phase showed that multi-grid approache provide robust and efficient convergence, while standard point-iterative solvers fail because of the 100:1 conductivity contrast. A particular sweet spot for thermal steering at $47.34^\circ$ fiber orientations is identified by the study. The findings verify that optimized directional alignment efficiently reroutes energy toward integrated radiators and avoid the sensitive material from burning or getting damaged.

## Contents

# 1 Introduction

## 1.1 Motivation

The need for extremely effective, lightweight, and passive heat control systems is what motivates the use of anisotropic Carbon Composite material in spacecraft thermal management. In contrast to conventional isotropic metals, Composite material enables thermal steering, which effectively shields delicate equipment from localized thermal loads by using the high longitudinal thermal conductivity of carbon fibers to direct heat flux along particular paths toward radiators. This structural-thermal integration removes the mechanical complexity of active cooling loops and drastically lowers mission mass

## 1.2 The Multiscale Approach: Overview of the transition from Micro-structural characterization (Phase 1) to System-level application (Phase 2).

A multiscale modeling approach is necessary for the design of sophisticated thermal management systems in order to close the gap between microscopic fiber configurations and macroscopic panel performance. To guarantee both physical consistency and numerical accuracy, this study is divided into two separate phases. In Phase 1, the micro-structural characterization of a Representative Volume Element (RVE) is the main focus. To capture how the steering angle $\theta$ and fiber volume fraction affect directional heat flow, the effective thermal conductivity tensor $\mathbf{K}_{eff}$ is derived by homogenizing the discrete fiber and matrix properties. In the study's second phase, the results are applied to a real-world engineering situation: a satellite radiator panel. During this stage, an electronic component that requires cooling is represented by a localized heat source in the panel. The objective is to see how the substance responds to a hot spot. The composite material is made to promote heat travel along the fiber paths, whereas standard materials permit heat to spread equally in all directions. As a result, a concentrated thermal energy trail known as a plume is produced, which travels from the heat source in the direction of the radiator edge. The study ascertains whether the heat can be purposefully steered toward a cooling interface by examining this plume.

### 1.2.1 Necessity

This multiscale approach is necessary because trying to simulate every single tiny fiber across a large $3$-meter panel would be impossible for even the fastest computers; it would require billions of mesh points. By splitting the problem into two phases, the complex behavior of the fibers is packaged into a single mathematical property called an equivalent continuum. This allows for a simulation that is fast enough to run multiple times while remaining accurate enough to show exactly how the material's internal structure can be tuned to meet a spacecraft's cooling needs. This proves whether the material's internal architecture can replace heavy cooling hardware by naturally directing thermal energy to where it can be safely released into space.

## 1.3 Project Scope

The project provides an automated Python pipeline to evaluate thermal steering through three main stages:

- Generating a refined grid in Gmsh that balances high resolution at heat interfaces with computational speed.

- Calculating the effective material properties by averaging the micro-scale heat flux within a representative sample.
- Solving the heat equation in FEniCS to quantify the drift and thermal performance of the full-scale radiator panel.

# 2 Phase 1: Material Homogenization (Micro-Scale)

**This section explains basics about composite material and how RVE is setup.**

## 2.1 Theoretical Framework: Anisotropy in Composite Material

A fiber-reinforced composite is a combination of two distinct materials: a uniform resin and a directional fiber reinforcement. The binding agent, which is isotropic by nature, is the resin. However, a directional component is added to the material properties by the addition of individual fibers, which are long, thin cylinders.

The composite is substantially more thermally conductive in the fiber direction than in the perpendicular directions due to this internal structure. This property characterizes the material as **anisotropic** [3]. As shown in Figure 1, these composites are specifically **orthotropic**, which means that their characteristics are defined along three perpendicular axes. as illustrated in Figure 1.

- **Direction 1 (Longitudinal):** This axis follows the length of the fibers. In this direction, heat conduction is at its peak because energy travels directly through the carbon filaments.
- **Direction 2 (Transverse):** This axis is perpendicular to the fibers but remains within the plane of the material.
- **Direction 3 (Through-Thickness):** Heat is moving up or down through the thickness of the panel.

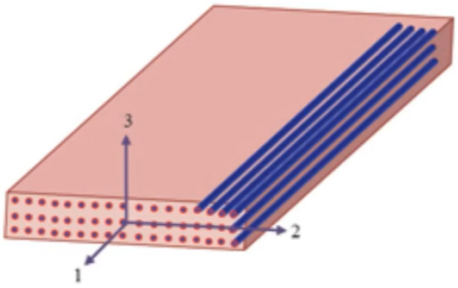


Figure 1: Unidirectional Composite material showing local coordinate axes.

## 2.2 Material Structure

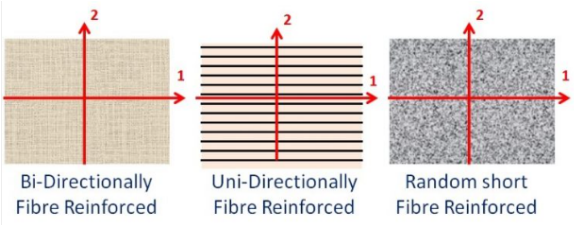


Figure 2: Directions of Composite Fibers

The uniform component of the composite is called the matrix (the glue). The nonuniform fiber stuff is called the reinforcement (Fibers).

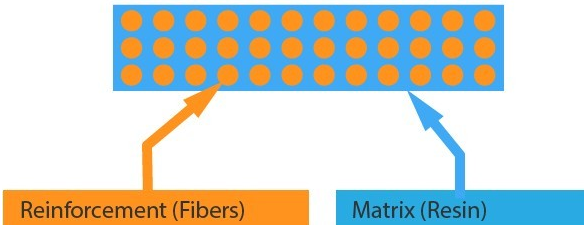


Figure 3: Reinforcement and Matrix

## 2.3 RVE Design and Smart Mesh Adaptive

The pipeline uses an automated Python generator to create the RVE while guaranteeing a conformal interface between the fibers and the resin in order to resolve the micro-scale geometry.

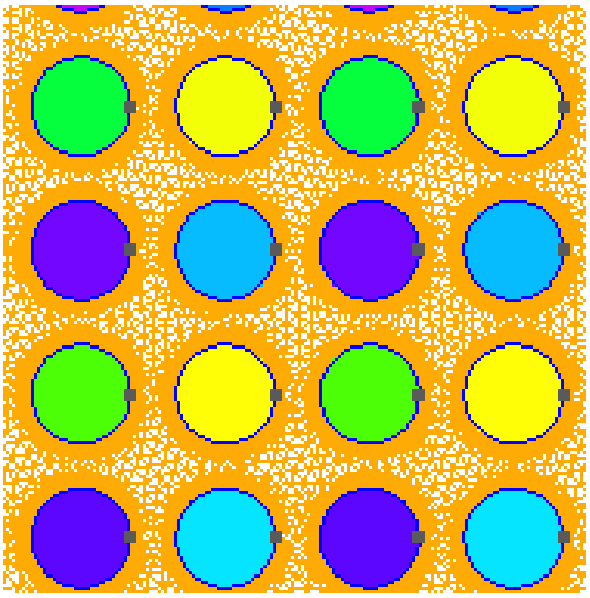

Figure 4: MESH Structure (Zoomed)

**Dual-Mode Safety Mechanism**

- **Manual Mode:** Fixed grid definition (e.g., $10 \times 10$).
- **Volume Fraction Mode:** Automatic fiber scaling to meet *target_vol_frac* while maintaining a *wall_gap* to prevent geometric overlaps.

Table 1: Configuration Settings

| Param | Role | Logic |
|---|---|---|
| $L$ | Domain Size | Defines unit RVE square boundary. |
| $R_{in}$ | Fiber Radius | Adjustable for manual/fraction runs. |
| $lc$ | Resolution | Base size of mesh elements. |
| $gap$ | Safety Margin | Prevents fiber-edge contact. |
| $V_f$ | Target Fraction | Optimizes fiber size for density. |

The system produces an unstructured mesh to capture curved fiber boundaries. This allows for local refinement at interfaces where temperature gradients are steepest. This smart refinement identifies the exact boundary where the fiber meets the resin and clusters smaller, more precise elements at that interface Figure 5. The code automatically switches to larger elements in the far-field regions where the physics is simpler. This greatly lowers the total number of computations the computer must do while guaranteeing that the most important regions for heat transfer the material interfaces are captured with high fidelity.

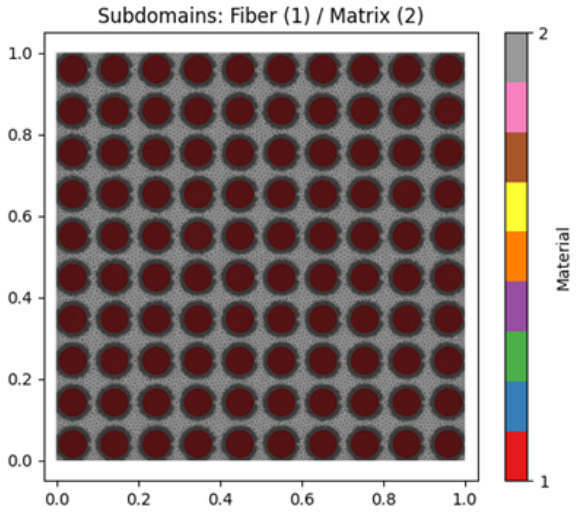


Figure 5: MESH Structure

## 2.4 Numerical Homogenization Theory And Mathematics

The goal of this subsection is to extract the bulk material properties of the composite. This process moves from the micro-scale physics of the fibers and resin to a single mathematical tensor.Within the RVE domain, where no internal energy is generated and the system is at steady state, the heat conduction is governed by the standard heat equation:

$$\nabla \cdot (\mathbf{K}(x, y)\nabla T) = 0 \tag{1}$$

Where: k = [W / (m ·K)]

T = Kelvin

### 2.4.1 Variational Formulation and the CG Method

To solve the steady-state heat equation on the RVE, The Continuous Galerkin (CG) method is employed. This finite element approach [5] ensures that the temperature values at the shared edges between the resin and the fibers are continuous. This reflects the reality because at the point of contact between two bodies, temperatures are the same. FEniCS 2019 is used to implement this in Python. The heat equation is solved in its variational (weak) form :

$$\int_{\Omega} \mathbf{K}(x, y)\nabla u \cdot \nabla v \, dx = 0 \tag{2}$$

Where:

- $u \in V$ is the trial function (Temperature $T$).
- $v \in V$ is the test function (Weighting function).
- K is the thermal conductivity.
- $f$ is the internal heat source.
- $\partial\Omega_N$ represents the Neumann boundary (heat flux $q$).

**Difference between FEniCS and OpenFOAM** It should be noted that FEniCS's approach is very different from OpenFOAM's, primarily because it replaces pre-configured black box solvers with explicit mathematical authorship. FEniCS necessitates a manual definition of the function space, such as the Continuous Galerkin method used here to guarantee temperature continuity across nodes, whereas OpenFOAM depends on the Finite Volume Method (FVM), which concentrates on cell-averaged fluxes and mainly conceals the nodal discretization from the user. This deliberate manualness ensures that the anisotropy is handled with nodal-level precision instead of using the generic non-orthogonal correctors usually needed in OpenFOAM.

FEniCS offers the transparency required to confirm that every facet of the physics from the conductivity derivation to the particular choice of the source term is mathematically consistent and directly controlled by the user, even though OpenFOAM might be easier to set up.

### 2.4.2 Rotation Tensor

Redrawing cylinders and regenerating the mesh for each angle $\theta$ is a conventional method of dealing with different fiber orientations. This brute force approach takes a long time and introduces numerical noise because the mesh quality varies slightly between iterations.Rather, the Rotation Tensor (RT) [7]is used in an optimized method. This RT allow us to change the fibers in direction we want without physically remeshing each time. In other words, using RT is physically identical to changing

direction of fibers in geometry taneously:

$$\mathbf{K}_{\text{rotated}} = \mathbf{R}\mathbf{K}_{\text{local}}\mathbf{R}^T$$

The rotation matrix $\mathbf{R}$ and the local diagonal tensor are defined as:

$$\mathbf{R} = \begin{bmatrix} \cos\theta & -\sin\theta \\ \sin\theta & \cos\theta \end{bmatrix}, \quad \mathbf{K_{local}} = \begin{bmatrix} k_{par} & 0 \\ 0 & k_{perp} \end{bmatrix}$$

Expanding the multiplication for each component:

- $K_{f,xx} : (k_{par} \cdot c)(c) + (-k_{perp} \cdot s)(-s) = k_{par}c^2 + k_{perp}s^2$
- $K_{f,xy} : (k_{par} \cdot c)(s) + (-k_{perp} \cdot s)(c) = (k_{par} - k_{perp})cs$
- $K_{f,yx} : (k_{par} \cdot s)(c) + (k_{perp} \cdot c)(-s) = (k_{par} - k_{perp})cs$
- $K_{f,yy} : (k_{par} \cdot s)(s) + (k_{perp} \cdot c)(c) = k_{par}s^2 + k_{perp}c^2$

As derived above, In the definition, $\alpha x'y$ is the cosine of the angle between the new $x'$ and the original $y$ .If it is rotated the x-axis toward the y-axis by an angle $\theta$:The angle between $x'$ and $x$ is simply $\theta$. So, $\alpha x'x = \cos(\theta)$.The angle between $x'$ and $y$ is $(90° - \theta)$.Using the trigonometric identity: $\cos(90° - \theta) = \sin(\theta)$ this rotation introduces these diagnol terms.

### 2.4.3 The Two-Simulation Approach

The relationship between the volume-averaged heat flux and the applied temperature gradient is defined by the effective conductivity tensor. To determine the heat flux at the micro-scale, the local flux $\mathbf{q}(x, y)$ is calculated at every integration point using the specific conductivities of the phases:

$$\mathbf{q}(x, y) = -\mathbf{K}(x, y)\nabla u(x, y) \qquad (3)$$

In this framework, $\mathbf{K}(x, y)$ represents the rotated anisotropic fiber tensor $\mathbf{K}_{\text{f}}$ for fiber domains and the isotropic matrix conductivity $k_{\text{m}}$ for the resin. The volume-averaged heat flux $\langle\mathbf{q}\rangle$ is then found by integrating these local fluxes over the RVE domain $\Omega$ [4]:

$$\langle\mathbf{q}\rangle = \frac{1}{|\Omega|}\int_{\Omega} \mathbf{q}(x, y)\, d\Omega \qquad (4)$$

$$\begin{bmatrix} \langle q_x\rangle \\ \langle q_y\rangle \end{bmatrix} = \begin{bmatrix} K_{xx} & K_{xy} \\ K_{yx} & K_{yy} \end{bmatrix} \begin{bmatrix} \Delta T_x \\ \Delta T_y \end{bmatrix}$$

where;

$$\mathbf{K}_{\text{eff}} = \begin{bmatrix} K_{xx} & K_{xy} \\ K_{yx} & K_{yy} \end{bmatrix} \qquad (5)$$

To populate the conductivity tensor, the framework executes two independent simulations by applying unit temperature gradients ($\Delta T = 1$).

**Simulation 1 (Horizontal Gradient):** $\Delta_x T = 1$ and $\Delta_y T = 0$ is set. The resulting volume-averaged heat fluxes provide the first column of the tensor:

$$\begin{bmatrix} \langle q_x\rangle \\ \langle q_y\rangle \end{bmatrix} = \begin{bmatrix} K_{xx} \\ K_{yx} \end{bmatrix}$$

**Simulation 2 (Vertical Gradient):** $\Delta_x T = 0$ and $\Delta_y T = 1$ is set. This reveals the second column of the tensor:

$$\begin{bmatrix} \langle q_x\rangle \\ \langle q_y\rangle \end{bmatrix} = \begin{bmatrix} K_{xy} \\ K_{yy} \end{bmatrix}$$

### 2.4.4 Symmetry Correction and Physical Consistency

The thermal conductivity tensor needs to be symmetric in accordance with Onsager's Reciprocal Relations [6]. This implies that the heat drift generated in the $x$-direction by a $y$-gradient should be the same as the drift generated in the $y$-direction by a $x$-gradient ($K_{xy} = K_{yx}$).There is a tiny discrepancy of $8.79 \times 10^{-3}$ between these two values in the simulation (here run for 10 degree). This occurs because the natural, free flow of heat

through the fibers is slightly disrupted by the imposition of Dirichlet boundary conditions, which fix the temperatures at the edges.

**Symmetry Validation and Resulting Tensor**

- **Pre-averaging Error ($|K_{xy} - K_{yx}|$):** $8.79 \times 10^{-3}$
- **Post-averaging Error:** $0.00 \times 10^{00}$

**Effective Conductivity Tensor:**

Periodic Boundary Conditions (PBC) would be a more accurate approach, but the current error is remarkably small, indicating that the simulation is already highly accurate.Both values are averaged to produce a perfectly symmetric tensor in order to maintain the physical behavior and guarantee mathematical stability. To preserve the physical behavior and ensure mathematical stability, both off-diagonal values are averaged to create a perfectly symmetric tensor:

$$K_{\text{eff},xy} = K_{\text{eff},yx} = \frac{K_{xy} + K_{yx}}{2} \tag{6}$$

## 2.5 Brief:Introduction to Solvers

**Pointwise smoothers.** Consider the linear system

$$Au = f, \tag{7}$$

where $A$ is a sparse symmetric positive (semi-)definite matrix arising from the discretization of an elliptic operator. Pointwise relaxation methods generate iterates

$$u^{k+1} = u^k + R(f - Au^k), \tag{8}$$

where $R$ is a simple approximation of $A^{-1}$, such as Jacobi or Gauss–Seidel. The corresponding error propagation is

$$e^{k+1} = (I - RA)e^k. \tag{9}$$

These methods effectively damp high-frequency error components but are inefficient for smooth error modes, particularly in the presence of strong coefficient contrasts.

**Multigrid principle.** Multigrid methods address this limitation by complementing smoothing with coarse-grid correction. Let $V$ denote the fine space and $V_c$ a coarse space. The prolongation operator

$$P : V_c \to V \tag{10}$$

maps coarse-grid corrections to the fine grid, while the restriction operator

$$R_c : V \to V_c \tag{11}$$

transfers residuals from the fine grid to the coarse grid. In the Galerkin framework, the restriction is defined as $R_c = P^\top$ and the coarse operator is

$$A_c = R_c A P = P^\top A P. \tag{12}$$

A two-level correction step then reads

$$u^{k+1} = u^k + P A_c^{-1} R_c (f - Au^k), \tag{13}$$

which efficiently reduces smooth error components that are poorly handled by the smoother.

**V-cycle construction.** The V-cycle algorithm is obtained by recursively applying the two-level correction across multiple grid levels. On each level, a small number of pre-smoothing steps reduces high-frequency error, the residual is restricted to a coarser space, the coarse problem is approximately solved, and the correction is prolongated back to the finer level. Post-smoothing is then applied to remove high-frequency errors introduced by interpolation. This recursive process yields a multilevel solver with convergence rates that are nearly independent of the problem size. The Figure 6 shows how restriction or shift to

coarser mesh is made in multi-grid solvers.

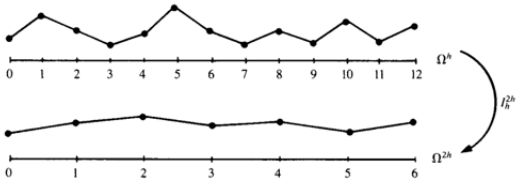


Figure 6: Restriction by full weighting of a fine-grid vector to the coarse grid

**GMG versus AMG.** In geometric multigrid (GMG), the spaces, prolongation, and restriction operators are defined using a hierarchy of meshes and finite element interpolation. Algebraic multigrid (AMG) constructs these operators directly from the matrix $A$, without geometric information. This makes AMG particularly effective for large, heterogeneous systems where a suitable geometric hierarchy is unavailable.

# 3 Phase 2: Satellite Panel Application

**This section details how obtained homogenized properties were used**

## 3.1 Preamble

The objective of this phase is to validate the practical application of the homogenized material properties calculated in Phase 1. While the previous section focused on the micro-scale interactions between fibers and resin, Phase 2 evaluates how these properties perform at a macro-scale system level.In this simulation, the effective conductivity tensor $\mathbf{K}_{\text{eff}}$ 5 is applied to a full-scale satellite radiator panel. In the following figure, it can be seen that the source term represents the electronic device to be saved from overheating, while the rest of the surface is the panel. It should be noted that both are composed of the same composite material.

## 3.2 Governing Equations for the Radiator Panel

The thermal behavior of the panel is governed by the steady state heat conduction equation. The domain is treated as a homogenized continuum. The strong form of the governing equation is:

$$-\nabla \cdot (\mathbf{K}_{\text{eff}} \nabla T) = f(x, y) \tag{14}$$

Where $f(x, y)$ represents the internal heat generation. Based on the domain markers in the mesh, this source term is defined piecewise:

$$f(x, y) = \begin{cases} Q & \text{in } \Omega_{\text{source}} \text{ (Tag 1)} \\ 0 & \text{elsewhere (Tag 2)} \end{cases} \tag{15}$$

### 3.2.1 Variational (Weak) Form

The equation is transformed into a variational form to be solved via the Finite Element Method [5] and [2]. This involves finding the temperature field $T$ such that for all test functions $v \in V$:

$$\int_{\Omega} \nabla v \cdot (\mathbf{K}_{\text{eff}} \nabla T)\, dx = \int_{\Omega_{\text{source}}} Q v\, dx \tag{16}$$

## 3.3 Boundary Conditions

The panel is designed as a controlled heat transfer system with the following constraints:

- **Heat Sink (Top Edge):** A Dirichlet boundary condition fixes the top edge at $T = 0$. This acts as the exit point for all thermal energy:

$$T = 0 \quad \text{on } \Gamma_{\text{top}} \tag{17}$$

- **Adiabatic Boundaries (Bottom and Sides):** Natural Neumann boundary conditions are applied to the remaining three edges, representing perfect thermal insulation ($\mathbf{q} \cdot \mathbf{n} = 0$):

$$-(\mathbf{K}_{\text{eff}} \nabla T) \cdot \mathbf{n} = 0 \quad \text{on } \Gamma_{\text{bottom}} \cup \Gamma_{\text{left}} \cup \Gamma_{\text{right}} \tag{18}$$

Heat is compelled to move upward by insulating the bottom and sides. Heat does not flow in a circle or a straight vertical line due to the fibers' preferential conduction pathways. Instead, targeted thermal management is made possible by the $K_{xy}$ term, which steers the heat plume diagonally. Without this configurations, heat will be trapped at insulation side, causing the sensitive device to be burned or damaged.

# 4 Results and Analysis

**This section explains result of simulations**

## 4.1 Phase 1 Results:Parametric Study of Fiber Orientation

This parametric study 7 serves as a critical validation of the code's physical accuracy by characterizing the effective thermal conductivity as a function of fiber orientation $\theta$.

- **Directional Trends:** As the fibers rotate, $K_{xx}$ (horizontal) and $K_{yy}$ (vertical) show inverse sinusoidal patterns, indicating that the model accurately tracks the alignment of the reinforcement.
- **Shear Coupling:** When fibers are not aligned with the coordinate axes, the maximum steering effect is accurately represented by the shear component $K_{xy}$, which peaks at $45°$.
- **Physical Consistency:** These curves' symmetry and smoothness throughout the $0°$ to $90°$ range attest to the numerical stability of the homogenization logic and finite element assembly. Grid-independence study was also conducted and results remained stable which is expected in this kind of geometry.

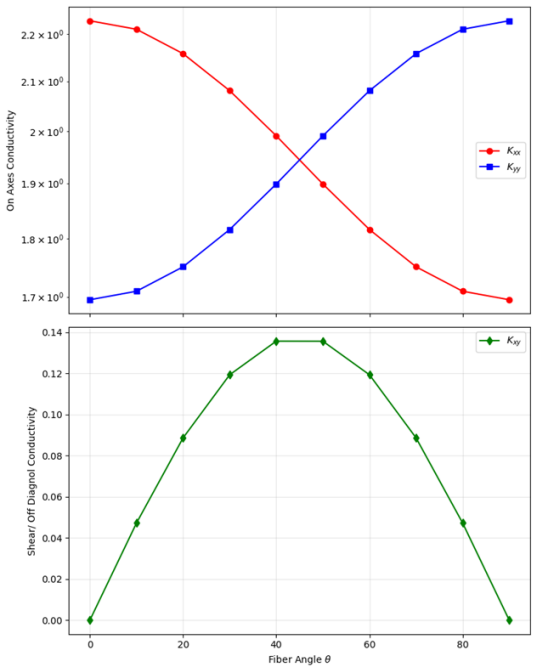


Figure 7: $K_{eff}$ Parametric study

### 4.1.1 Horizontal Temperature Gradient

The figure 8 shows the temperature when horizontal gradient is applied. It can be clearly seen that temperature values close to left side of boundary quickly becomes zero because of Dirichlet condition applied which give the symmetry error. However,

this small error is catered in an efficient way as previously discussed in the Phase 1 section.

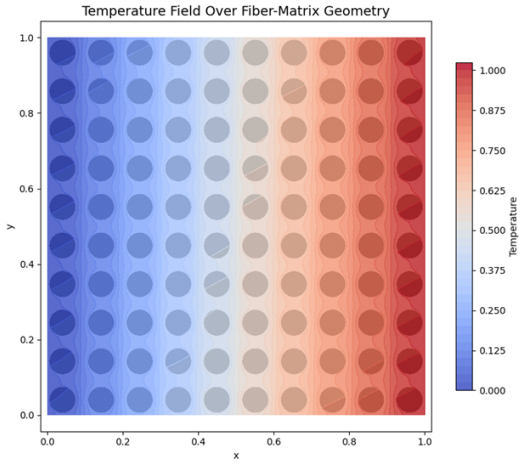


Figure 8: Horizontal Temperature Gradient

### 4.1.2 Numerical Stagnation in Heterogeneous Media

The mathematical structure of the coefficient matrix $A$ is directly responsible for the failure of basic iterative solvers. The connectivity and thermal resistance between each mesh node are represented by $A$ in this finite element context. The matrix becomes numerically unbalanced when material properties differ by a factor of 100 (for example, $k_{fiber}$ vs. $k_{matrix}$).

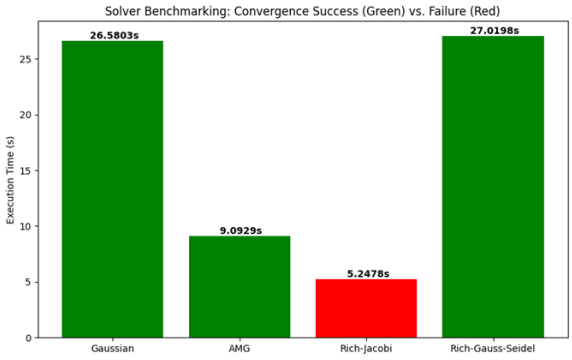


Figure 9: Solver Performance Comparison: Computational time and convergence status for different iterative and direct methods.

**Coefficient Matrix Structure and Conditioning**

The matrix $A$ is assembled from local contributions, leading to a stark contrast in row magnitudes:

- **Matrix Rows ($k_m = 1$):** Nodes within the matrix produce relatively small numerical values.
- **Fiber Rows ($k_{fiber} = 100$):** Nodes within the fiber produce values roughly 100 times larger.

This disparity results in a high **condition number**, characterizing the matrix as stiff. [1]

**Update Bottleneck in Point-Iterative Solvers**

The Jacobi and Gauss-Seidel methods solve for the temperature $u_i$ at iteration $k+1$ by isolating the diagonal entry $A_{ii}$. Consider jacobi method and Gauss-Seidel :

$$u_i^{(k+1)} = \frac{1}{A_{ii}} \left( b_i - \sum_{j \neq i} A_{ij} u_j^{(k)} \right) \tag{19}$$

$$x_i^{(k+1)} = \frac{1}{a_{ii}} \left( b_i - \sum_{j<i} a_{ij} x_j^{(k+1)} - \sum_{j>i} a_{ij} x_j^{(k)} \right) \tag{20}$$

For nodes located within the high-conductivity fiber, $A_{ii}$ is very large. Consequently, the correction term is divided by this large value, rendering the temperature update $\Delta u$ extremely small. This phenomenon, known as **Local Stagnation**, causes the solver to perform thousands of iterations with only microscopic changes to the solution. In the Figure 9, it can be seen that Gauss-Seidel(GS) struggles to reach convergence. The reason is again the diagonal term, making the update of solution slower. However, (GS)

uses the updated value from current iteration $x_j^{(k+1)}$ which makes it more stable and successful than Jacobi's method.

AMG overcomes numerical stiffness by mathematically averaging the high-contrast conductivity values at coarser levels. While the fine mesh is trapped by the sharp $100:1$ cliffs between fiber and matrix, the coarsening process blends these regions into macro-blocks with uniform, effective properties. This removes the local bottlenecks, allowing heat information to flow globally across the domain in a single V-cycle.

## 4.2 Phase 2 Thermal Mapping Results

In order to see how much heat is driven away from the sensitive electronic material (Source) shown in the Figure 10, a Heat map is drawn, which clearly shows the expansion of temperature values from the source. There has been various maps drawn for the fibers at different angles in the Project Phase 2 (.ipynb). However, for the illustration see the following figure

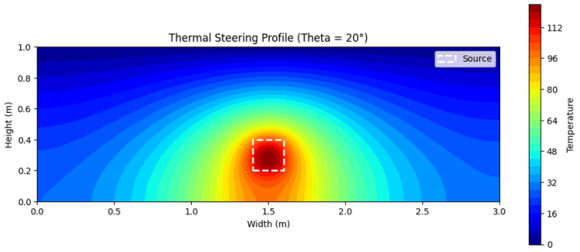


Figure 10: Panel and Source(electronic device)

### 4.2.1 Peak Drift Quantification

The Figure 11 top edge of the panel has a Dirichlet Boundary Condition set to $0°$C. This boundary functions as a radiator or physical heat sink. It forces the heat generated by the source at the bottom to travel upward through the composite material before being dissipated at this edge. The y-axis represent the temperature at 90 percent of height of panel and the center dashed line at $1.5$ m represents the geometric symmetry axis, which is also the exact midpoint of the heat source.

At angle $0°$, the diagonal terms of conductivity are zero, which means there is no significant steering effect. The negative draft show heat moved to left of center source or symmetrical axis. As soon as the fibers are rotated, the steering effect becomes significant. In other words, heat starts to flow in a preferential direction, which avoids accumulation in the edges around the sensitive device.

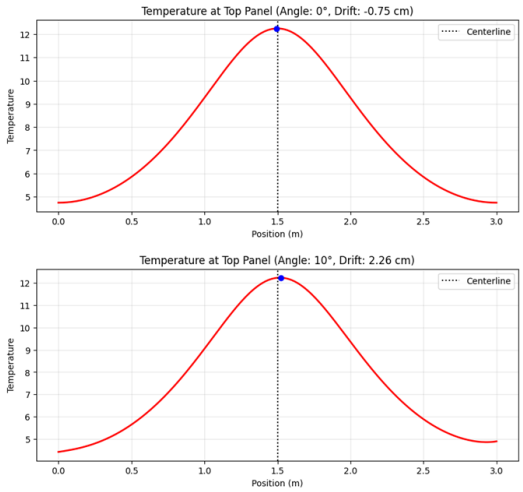


Figure 11: Drift Upon Changing Angles)

$$\delta = x_{max} - x_{center} \tag{21}$$

### 4.2.2 Maximum Steering

The Figure 12 give relation between angles and drift. It can be seen from the figure that drift of heat remains constant at angles from 20 till 60. Further tilting of fibers start to reduce this steering effect. Giving the indication that there is more than one sweet spot. However, What does the code is that its finding the max temperature at 90% of top edge height. When the angle is tilted, heat flux is beamed at the targeted edge height. By tilting fibers, the beam of heat flux may narrow or broaden,

but it may not move away from certain coordinates x where it gives the max temperature.

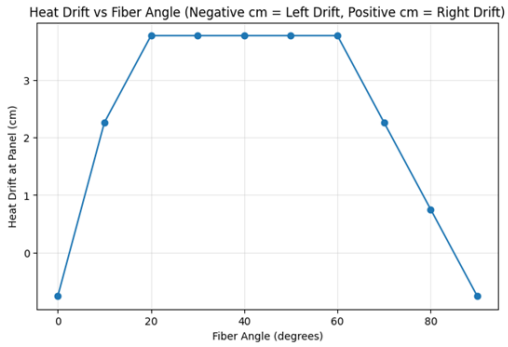


Figure 12: Drift Upon Changing Angles

In order to get the optimum angle to protect device, Average temperature near source and top panel edge for various angles is considered Figure 13. The dashed green line at $47.34°$ identifies the sweet spot. At this angle, the system achieves the best balance: it utilizes the maximum steering capability of the $K_{xy}$ term (which peaks at $45°$) to move heat diagonally while maintaining enough vertical conductivity ($K_{yy}$) to prevent heat accumulation around the source.

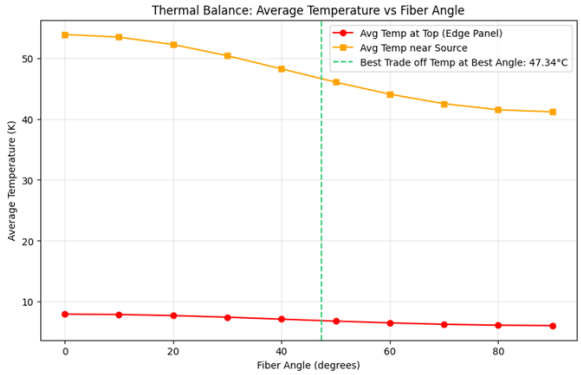


Figure 13: Average Temperatures Vs Fiber Angles

# 5 Conclusions

This study effectively shows that multiscale homogenization is a very effective method for modeling very complex thermal steering with greatly lowering computational expenses without sacrificing physical accuracy. The numerical framework revealed that standard point-iterative solvers fail due to the $100 : 1$ conductivity contrast, whereas advanced multiscale methods ensured robust convergence. By centering the heat source at the $1.5$ m axis, the model confirmed geometric symmetry and quantified a specific sweet spot for thermal management $47.34°$ fiber orientations. These findings demonstrate that heat is trapped around delicate electronic devices in the absence of optimized fiber tilting; however, energy can be diverted from crucial space components and directed toward the heat sink by using the oriented fibers.

# References

[1] Claude Brezinski. "Regularization of Ill-Conditioned Systems". In: *Computational Aspects of Linear Control*. Ed. by Claude Brezinski. Vol. 1. Numerical Methods and Algorithms. Springer, Boston, MA, 2002, Chapter 9. ISBN: 978-1-4613-0261-2. DOI: 10.1007/978-1-4613-0261-2_9.

[2] FEniCS Project. *DOLFIN Python API Reference (Version 2019.1.0)*. Accessed: 2026-01-24. The FEniCS Project. 2019. URL: https://olddocs.fenicsproject.org/dolfin/2019.1.0/python/.

[3] Ronald F. Gibson. *Principles of Composite Material Mechanics*. 4th. Mechanical Engineering. See pp. 27–40 for material structural hierarchy and pp. 44–50 for industrial applications. CRC Press, 2016. ISBN: 978-1-4522-5039-1.

[4] Behrooz Hassani and Ernest Hinton. *Homogenization and Structural Topology Optimization: Theory, Practice and Software*. See pp. 55–66 for approximation of conductivity via RVE averaging. Springer London, 1999. ISBN: 978-1-4471-1229-7. DOI: 10.1007/978-1-4471-0891-7.

[5] Hans Petter Langtangen and Kent-Andre Mardal. *Introduction to Numerical Methods for Variational Problems*. Texts in Computational Science and Engineering. Foundational text for finite element implementation in FEniCS. Springer Cham, 2019. ISBN: 978-3-030-23787-5. DOI: 10.1007/978-3-030-23788-2.

[6] Lars Onsager. "Reciprocal Relations in Irreversible Processes. I." In: *Physical Review* 37.4 (1931). Foundational paper for the symmetry of transport tensors., pp. 405–426. DOI: 10.1103/PhysRev.37.405.

[7] C. F. Yang and L. J. Qin. "Graphical Representation and Explanation of the Conductivity Tensor of Anisotropic Media". In: *Surveys in Geophysics* 41.2 (Jan. 2020). Theoretical basis for the visualization and rotation of conductivity tensors., pp. 249–281. DOI: 10.1007/s10712-019-09581-5.